Modeling and Simulation of Photovoltaic Modules Using Bio-Inspired Algorithms

Lucas Lima Provensi, Renata Mariane de Souza, Gabriel Henrique Grala, Rosângela Bergamasco [ID]**, Rafael Krummenauer** [ID] **and Cid Marcos Gonçalves Andrade *** [ID]

Department of Chemical Engineering, State University of Maringa, Maringa 87020-900, PR, Brazil; llprovensi@uem.br (L.L.P.); pg54842@uem.br (R.M.d.S.); gabrielgrala@gmail.com (G.H.G.); rbergamasco@uem.br (R.B.); rkrummenauer2@uem.br (R.K.)
* Correspondence: cmgandrade@uem.br; Tel.: +55-44-3011-4778

Abstract: This research aims to employ and qualify the bio-inspired algorithms: Particle Swarm Optimization (PSO), Genetic Algorithm (GA), and Differential Evolution Algorithm (DE) in the extraction of the parameters of the circuit equivalent to a photovoltaic module in the models of a diode and five parameters (1D5P) and two diodes and seven parameters (2D7P) in order to simulate the I-V characteristics curves for any irradiation and temperature scenarios. The peculiarity of this study stands in the exclusive use of information present in the module's datasheet to carry out the full extraction and simulation process without depending on external sources of data or experimental data. To validate the methods, a comparison was made between the data obtained by the simulations with data from the module manufacturer in different scenarios of irradiation and temperature. The algorithm bound to the model with the highest accuracy was DE 1D5P, with a maximum relative error of 0.4% in conditions close to the reference and 3.61% for scenarios far from the reference. On the other hand, the algorithm that obtained the worst result in extracting parameters was the GA in the 2D7P model, which presented a maximum relative error of 9.59% in conditions far from the reference.

Keywords: photovoltaic module; bio-inspired algorithms; modelling; parameter extraction; simulation

1. Introduction

The great technological development, changes in habits, and needs of the society of the 21st century propelled a growing global demand for energy. In addition, the scarcity of fossil fuel stocks and the environmental impacts generated by non-renewable energies intensify the world's interest in renewable, sustainable, and clean energy sources [1,2] coming from biomass [3], bioethanol [4], wind [5], and photovoltaic [6].

Among the renewable energy sources, solar energy stands out, which is captured and transformed by photovoltaic (PV) panels. The number of installed photovoltaic systems has shown a significant increase, as shown by [1], which reveals that at the end of 2018, more than 500 GW of power generated by photovoltaic panels was reached worldwide. Four years later, in 2022, the mark of 1 TW global solar capacity was achieved [7]. Also, according to the authors, it is estimated that in the year 2030, this will be 10 TW, and in 2050, 70 TW of power will be generated by photovoltaic panels, thus supplying a large part of the global energy consumed.

Although in recent years there have been public concessions with reduced fees and taxes, investment in technological advances, and improvements in efficiency and in the capacity of energy produced, which have led to a significant reduction in system costs, the grouping of photovoltaic equipment still presents a costly acquisition, installation, and engineering cost [8], especially in large installations such as power plants.

In this sense, studies and simulations between the photovoltaic generation system and its installation area, together with the detection of possible failures in energy generation

or tracking systems, can increase the precision in dimensioning and consequently avoid economic losses [9,10].

Note that, for a good simulation, other factors are taken into account, in particular, the environmental and climatic factors (e.g., temperature and irradiation) as well as the model of the photovoltaic panels that are responsible for emulating the behavior of the PV in the values of current and voltage outputs I × V under real operating conditions in order to evaluate the performance of the system in specific meteorological conditions of a certain region or even in conditions unfavorable to the generation of energy [11].

Thus, modeling the energy production of a photovoltaic module occurs through simulations of photovoltaic electrical characteristics, which are modeled by an equivalent electrical circuit [12]. Several types of equivalent circuit models have been proposed over the years, among which stand out the single-diode models [10,12,13] and two diodes [14–16].

To extract the parameters of the PV model, mathematical or computational methods are used to solve non-linear equations [17]. There is a wide variety of optimization techniques that are used in the extraction of parameters, among which is the use of heuristic algorithms, such as the Genetic Algorithm (GA), Particle Swarm Optimization (PSO), and the Differential Evolution Algorithm (DE), among others [16].

According to [11,18], the greater the number of diodes, the more accurate the simulation can be but the greater the number of parameters to be estimated. Thus, with the increase in the order of the model, there is inevitably an increase in its flexibility, making it more susceptible to overfitting concerning the scarce reference data. Another issue, much less critical but not irrelevant, is the increase in computational cost to solve the model's regression problem.

Several studies that apply heuristic algorithms for PV simulation add a wide variety of current-voltage (I × V) data external to the datasheet [10,19–21]. These external data can be obtained in the following ways: experimentally with field measurements, by pre-existing simulations of the module, and using external studies carried out previously [13]. The choice of approach can make the simulation process costly or even unfeasible. In this context, this work stands out for its ability to employ bio-inspired algorithms without needing external information added to the module's datasheet.

Thus, the objective of this work is to simulate and evaluate the performance of PV modules under different environmental conditions of irradiation and temperature in the models of one diode and five parameters (1D5P) and two diodes and seven parameters (2D7P), using bio-inspired algorithms such as PSO, GA, and DE in extracting the parameters of the equivalent circuit equations, using only the data provided in the Canadian manufacturer's datasheet [22].

The manuscript is organized as follows: Section 2 presents the materials and methods. It starts with Section 2.1, which describes two electric circuit models that are equivalent to the photovoltaic module and their respective equations and parameters to be extracted. In the next section, bio-inspired optimization methods are presented, beginning with the concepts of the fitness function common to all methods in Section 2.2. Section 2.3 details how each method is constructed for extracting the parameters in the reference conditions. With the extracted parameters, Section 2.4 reveals how the parameters are employed for generating the curves I × V. Section 3 presents, firstly, the values of the parameters extracted from each combination of a model with a bio-inspired method and advances to the I × V curves in five different conditions of temperature and irradiation, each figure is accompanied by a table that contains essential points of the graph. Finally, the last section is the conclusion, which summarizes the results obtained and the implications of the findings.

2. Materials and Methods

2.1. Equivalent Circuit Models of the Photovoltaic Cells

A photovoltaic module is formed by several photovoltaic cells connected in series. In turn, the photovoltaic cell is the device capable of performing the photovoltaic effect, which consists of transforming the energy of solar radiation into electrical energy. The

most used material for constructing commercial photovoltaic modules are those with monocrystalline silicon and polycrystalline silicon [23,24]. To realize the modeling process of a photovoltaic panel, it is necessary to determine the parameters that represent the physical phenomena verified in the equipment. For this purpose, it is necessary to establish an electrical model equivalent to a real model. This process is crucial because it allows for estimating precisely the energy produced by the module as well as the electrical parameters for any conditions [13].

According to [25], the behavior of a photovoltaic cell can be represented by an equivalent electric circuit that contains an electric current source in parallel with a diode. The current source is responsible for generating a continuous electric current, and the diode represents the PN junction of the semiconductor contained within the photovoltaic cells, which is responsible for generating the saturation currents [26]. Though, an equivalent circuit with only these two components is not enough to represent the I × V curve of a real photovoltaic panel [27] since the ohmic losses of the material and the internal cell dissipation are not considered. Thus, the most common models in the literature to represent a commercial photovoltaic cell are based on a current source connected to one or two diodes and resistors to represent ohmic losses and dissipation. Many authors classify the models by the number of diodes in the equivalent circuit and the number of parameters to be extracted. Based on this convention, the most used models of photovoltaic cells are one diode and five parameters [10,13] and two diodes and seven parameters [14,28].

2.1.1. The Single-Diode PV Model

The single-diode model is one of the most widely utilized equivalent electric circuit models in the literature for representing a photovoltaic cell [11,29]. According to [20], a photovoltaic cell is composed of a photo-generated current (I_L), which is produced by the flow of light that generates a continuous electric current and by its resistances, being produced in series by the semiconductor material itself in its metallic contacts and the resistance in parallel represents an alternative path for the flow of electric current caused by impurities or defects in the cell. Thus, the model of a single-diode (SDM) can represent the photovoltaic cell, consisting of an ideal diode connected in series with a current source, which represents the photo-generated current, and the two resistances that demonstrate the losses, being the resistance in series (R_s), and shunt resistance (R_{sh}) [30], as shown in Figure 1.
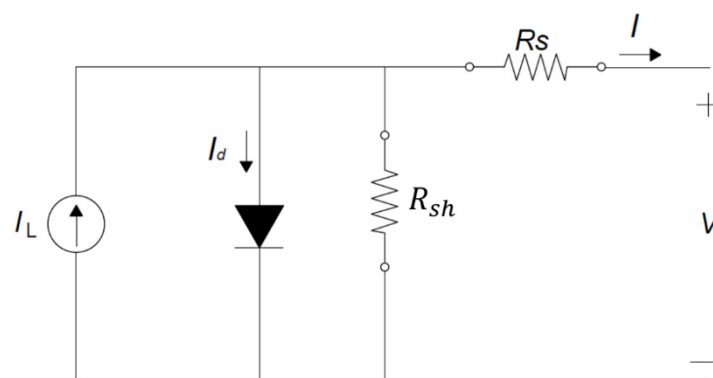

Figure 1. Equivalent circuits of the single-diode model.

Thus, the result is five unknown parameters to be extracted in this model, namely: the ideality factor of the diode (A), the reverse saturation current of the diode (I_0), the photo-generated current (I_L), the series resistance (R_s), and the resistance in parallel (R_{sh}).

The five parameters to be obtained are present in the SDM characteristic equation, obtained from Kirchhoff's law, and express the electric current as follows.

$$I = I_L - I_d - \frac{V + Rs\,I}{Rsh} = I_L - I_0\left[exp\left(\frac{q(V + IRs)}{AkT_c}\right) - 1\right] - \frac{V + Rs\,I}{Rsh} \tag{1}$$

where I is the cell output current (A); I_d is the current flowing through the diode (A); I_0 is the inverse saturation current of the diode (A); q is the elementary charge of the electron (1.602×10^{-19} coulombs); k is the Boltzmann constant (1.31×10^{-23} J K^{-1}); Tc is the cell temperature (K); A is the diode ideality factor, and V is the cell output voltage (V).

Because PV consists of several photovoltaic cells connected in series (N_{CS}), Equation (1) became:

$$I = I_L - I_0 \left[exp\left(\frac{q(V + IRs)}{N_{CS}AkT_c} \right) - 1 \right] - \frac{V + Rs\, I}{Rsh} \tag{2}$$

Thus, Equation (2) is used to extract the five parameters of the 1D5P model. Although this model describes the photovoltaic cell very well, it disregards the effect of loss of recombination current in the depletion area [30]. Furthermore, according to [31] and the authors [29], the single-diode model presents inaccuracy in the modeling under low illumination conditions.

Therefore, to correct such inaccuracies, one more diode was included in the modeling, thus constituting the double-diode model (DDM), also called 2D7P, as discussed in the next section.

2.1.2. The Double-Diode PV Model

From the double-diode model, it is possible to simulate the recombination effect of the special load, adding a separate current component with its exponential voltage dependence. Thus, in some cases, the literature demonstrates that this model presents greater simulation accuracy than the single-diode model [15,18,29]. Figure 2 shows the equivalent electrical circuit of the double-diode model.
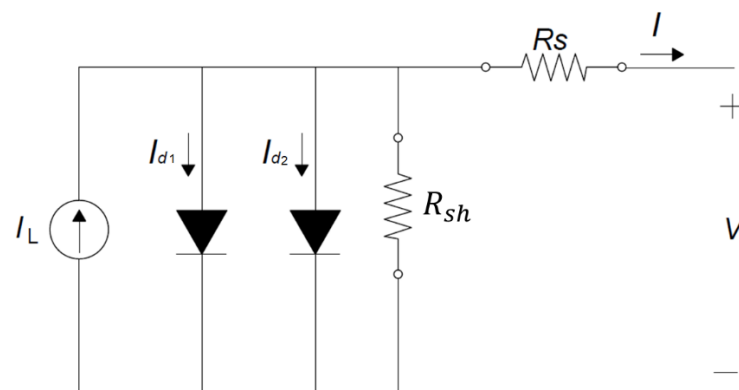

Figure 2. Equivalent circuits of the double-diode model.

Note that when adding another diode in the equivalent electrical circuit, there is an increase in the number of parameters to be found. Thus, in addition to the five parameters of the single-diode model, this model requires the extraction of two additional parameters, namely: the diode ideality factor of the second diode ($A2$) and the inverse saturation current of the second added diode (I_{02}), calling the model 2D7P.

Thus, the equation representing the circuit will be:

$$I = I_L - I_{01} \left[exp\left(\frac{q(V + IRs)}{A1kT_c} \right) - 1 \right] - I_{02} \left[exp\left(\frac{q(V + IRs)}{A2kT_c} \right) - 1 \right] - \frac{V + Rs\, I}{Rsh} \tag{3}$$

Analogously to what was completed in the Equation for the SDM, due to the numerous cells connected in series, Equation (3) becomes:

$$I = I_L - I_{01} \left[exp\left(\frac{q(V + IRs)}{A1N_{CS}kT_c} \right) - 1 \right] - I_{02} \left[exp\left(\frac{q(V + IRs)}{A2N_{CS}kT_c} \right) - 1 \right] - \frac{V + Rs\, I}{Rsh} \tag{4}$$

From Equations (2) and (4), bio-inspired optimization algorithms are applied to obtain the parameters.

2.2. Initial Concepts for Extracting Parameters

Regardless of the bio-inspired algorithm to be applied, some concepts are common between the methods. For example, candidate to be the solution to the problem is called an individual, in this case, the parameters to be extracted. Thus, it is called a population, a set of individuals.

The first step for extracting parameters by bio-inspired algorithms is randomly generating an initial population of Np individuals. However, some restrictions are applied. These primarily determine the intervals in which the parameter values are physically possible. If there is enough information, further restrict these ranges to values most likely to occur. Table 1 shows the ranges of values for each parameter for both models [13].

Table 1. Parameter ranges for the initial population of a 1D5P and 2D7P for Particle Swarm Optimization, a Genetic Algorithm, and a Differential Evolution Algorithm.

Parameters	Minimum	Maximum
I_L	$0.90 \times I_{iscref}$	$1.10 \times I_{iscref}$
I_0 or I_{01} and I_{02}	10^{-8} A	10^{-5} A
A or $A1$ and $A2$	1	2
R_s	$0\ \Omega$	$10\ \Omega$
R_{sh}	$1000\ \Omega$	$5000\ \Omega$

In this work, the standard test conditions (STC) will be used as a reference, given that it is possible to find all the values of the main points of the I $\times$ V curve for this condition in the datasheet of a module. The terms that appear with "*ref*" are those obtained from the manufacturer's data sheet under standard conditions.

Another important and common operation in all algorithms of this work is the criteria for evaluating individuals. This criterion, called the fitness function (*ff*), aims to check whether the parameters fit the model. This function starts from the equation of the equivalent circuit. In this sense, Equation (2) is used for the case of 1D5P, and for the 2D7P model, it is established by Equation (4). In order to build the fitness function, it is necessary to set the model equation equal to zero and to apply it to each of the points found in the module's datasheet under the reference conditions, namely, the open circuit voltage (V_{0Cref}, 0), maximum power point (V_{MPref}, I_{MPref}) and short-circuit current (0, I_{SCref}). Substituting the obtained data and the physical constants, the system will present three equations, where the unknowns will be only the parameters the algorithm needs to extract.

To keep the values always positive, the Root Mean Square Error (RMSE) criterion is used. As the name implies, this criterion consists of adding the square of each side of the equations that are not zero, and the result of the sum is divided by the number of equations, after which the square root is taken in the result obtained, as shown in Equation (5). Consequently, Equations (6) and (7) mathematically show the fitness function for the cases of 1D5P and 2D7P, respectively.

$$\text{RMSE}(x) = \sqrt{\frac{1}{N}\sum_{k=1}^{N} ff(V,I,x)2} \tag{5}$$

where N is the number of experimental points used; ff is the fitness function referring to the model to be employed.

$$ff(V,I,x) = I_L - I_0\left[exp\left(\frac{q(V+IR_s)}{N_{cs}AkT_c}\right) - 1\right] - \frac{V+Rs\,I}{Rsh} - I \tag{6}$$

where $x = \{I_L, I_0, A, R_S, R_{sh}\}$ for the $1D5P$ model.

$$ff(V, I, x) = I_L - I_{01}\left[exp\left(\frac{q(V + IR_s)}{N_{cs}A1kT_c}\right) - 1\right] - I_{02}\left[exp\left(\frac{q(V + IR_s)}{N_{cs}A2kT_c}\right) - 1\right] - \frac{V + RsI}{Rsh} - \text{I} \tag{7}$$

where $x = \{I_L, I_{01}, I_{02}, A1, A2, R_S, R_{sh}\}$ for the 2D7P model.

Once the initial population intervals and the evaluation criteria are established, each algorithm extracts the parameters according to Section 2.3.

2.3. Bio-Inspired Algorithms

2.3.1. Particle Swarm Optimization (PSO)

Proposed by James Kennedy and Russell C. Eberhart in 1995, the optimization algorithm starts from the idea of reproducing on a computer how societies process knowledge [32].

In this algorithm, the individual is called a particle. Thus, each particle has D information. Such information represents the parameters to be found. It is xi, a position vector belonging to $\mathbb{R}^D$ that represents the position of the particle, and vi, a velocity vector belonging to $\mathbb{R}^D$ that characterizes the vector velocity and indicates the direction of the particle's movement. The next position of the particle is given by Equation (8).

$$xi\,(t + 1) = xi\,(t) + vi\,(t + 1) \tag{8}$$

where $xi(t)$ is the current position of the particle and $vi(t + 1)$ is described by Equation (9):

$$vi(t + 1) = 0.729 \cdot [vi(t) + \psi1 \cdot (pi(t) - xi(t)) + \psi2 \cdot (pg(t) - xi(t))] \tag{9}$$

Therefore, $vi(t)$ is the velocity in the previous iteration; $pi(t)$ is the best position visited by the particle so far; $pg(t)$ is the best position found by any member of its neighborhood in the current iteration; and $\psi1$ and $\psi2$ are positive random vectors whose elements are generated from a uniform distribution with predefined upper bounds as follows: $\psi1 \sim U(0, L1)$ e $\psi2 \sim U(0, L2)$, where $L1 = L2 = 1.49445$ [19]. Because Equation (11) is multiplied by the factor 0.729, this algorithm is a variant of the traditional PSO, which is called Particle Swarm Optimization with constriction factor [33].

For extracting the parameters, the first step is the generation of the initial population, which is carried out in a pseudo-random manner, with $Np = 50$ and intervals provided by Table 1, as discussed in Section 2.2. Subsequently, each particle is evaluated by *ff*, and the algorithm advances according to the flowchart shown in Figure 3. Afterward, finding the values of *pi* and *pg* and updating the values of *xi* and *vi*, described in Equations (8) and (9), respectively. This recursion is performed until the stopping criterion is activated. In this research, this was a total of 1000 generations (*Ng*). The *Np* and *Ng* values are justified in the parameter fine-tuning revealed in Section 3.1.

Finally, the individual of the last generation with the lowest fitness value is determined. The individual's information will be the parameters that the algorithm needs to find.

2.3.2. Genetic Algorithm (GA)

John Holland developed the Genetic Algorithm in 1975, proposing an optimization algorithm that uses Charles Darwin's evolutionary theory as a metaphor for natural selection and reproduction processes to reproduce such ideas in the computer [34].

In this case, the candidate to solve the problems is called a chromosome or individual. Each chromosome has M information, representing the parameters to be found. Analogously to the PSO, the first step is the generation of the initial population, which is conducted pseudo-randomly, with Np = 50 and intervals provided by Table 1. Subsequently, each particle is evaluated by *ff*, and the algorithm advances according to the flowchart in Figure 4, with the operators: Selection GA, Crossover GA, and Mutation GA, described in the corresponding Sections below. This recursion is performed until $Ng = 3000$. The *Np* and *Ng* values are justified in the parameter fine-tuning revealed in Section 3.1.
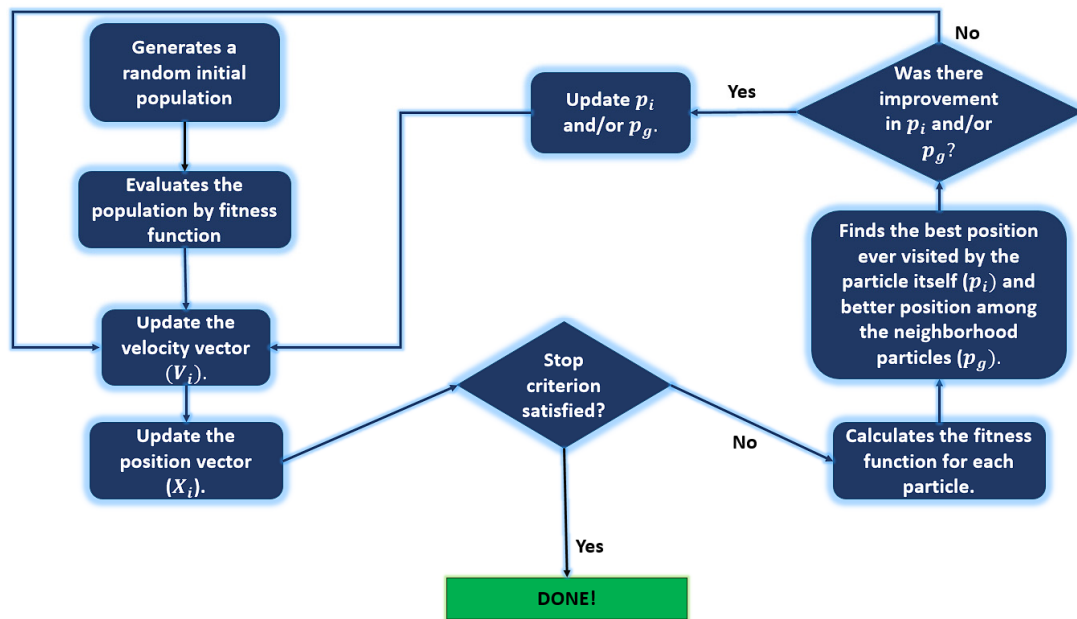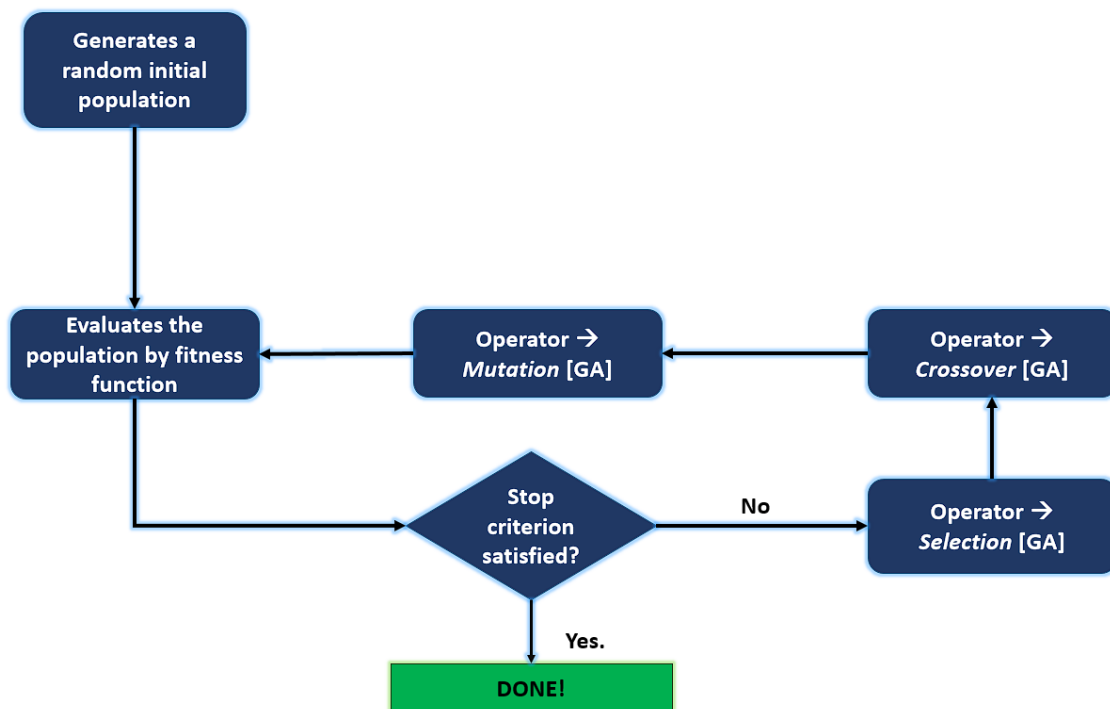
Figure 3. Flowchart for PSO.

Figure 4. Flowchart for GA.

Finally, the individual of the last generation with the lowest fitness value is determined. The individual's information will be the parameters that the algorithm needs to find.

Selection Operator for GA

According to [35,36], the tournament method is one of the main methods used for the selection operator. In short, this operator is implemented as follows: N_t individuals are extracted from the temporary population, forming the set P_t, which will be the individuals that will compete in the tournament. The tournament winner will be the individual from the P_t set with the lowest fitness value. Thus, this individual is inserted into the population for the next iteration. This procedure is repeated Np times to complete the population.

Crossover Operator for GA

Crossover is the operator based on the sexual reproduction of living beings, and its purpose is to create children by mixing the genetic characteristics of the parents selected in the previous operator. For this, P_c is defined as the crossover probability parameter, which defines the probability of an individual being selected for this purpose. Thus, in each iteration, N_f individuals from the population are chosen. Within this set, pairs are formed to generate descendants with the recombined chromosomes [37].

The arithmetic crossover method is used to carry out the combination of chromosomes [38]. According to the authors, the descendants are formed from linear combinations of the original individuals. Therefore, if $x_g = [x_1 \ldots x_m]^M$ and $y_g = [y_1 \ldots y_m]^M$ are two individuals selected for reproduction, the components of the new individuals will be obtained according to Equations (10) and (11), respectively.

$$x_{gi} = \alpha_g x_{gi} + (1 - \alpha_g) \times y_{gi} \tag{10}$$

$$y_{gi} = (1 - \alpha_g) \times x_{gi} + \alpha_g y_{gi} \tag{11}$$

where α_g is a random real number between 0 and 1, $\alpha_g \sim U(0,1)$. Once the descendants are generated, they are added to the original population, forming a temporary population subjected to the mutation process.

Mutation Operator for GA

This genetic operator aims to add genetic characteristics to the individuals of the population. This process is controlled by a fixed parameter P_M, called mutation probability, recommended as 1% [39]. According to [40], a widespread way to use the operator is as follows: if it is a real vector $r = [r_1 r_2 \ldots r_M]$, a prevalent way to generate a descendant $r' = [r_1' \ldots r_M']$ per mutation is given by Equation (12).

$$r_j' = r_j + m_j \tag{12}$$

where j denotes the jth component of r that was selected for mutation, and m_j is a random variable. Using a normal (Gaussian) distribution, with zero mean and variance σ_m, has been one of the main ways to introduce mutation in real coding individuals.

2.3.3. Differential Evolution Algorithm (DE)

The optimization method called differential evolution was proposed by J. Storn and K. Price in 1995 with the idea of creating a metaheuristic population dedicated to the optimization of functions in continuous spaces, that is, for parameters with values belonging to the group of real numbers [41,42]. The steps of this algorithm are similar to the Genetic Algorithm. However, the peculiarity of this technique lies in the use of information present in the population itself to introduce disturbances in individuals [40].

In this algorithm, the individual is also called the target vector and has D information, the parameters to be extracted. Analogously to the other algorithms, the first step is the generation of the initial population, which is conducted pseudo-randomly, with $Np = 50$ and intervals provided by Table 1. Subsequently, each particle is evaluated by ff, and the algorithm advances according to the flowchart in Figure 5, with the operators' Mutation DE, Crossover DE, and Selection DE described in the corresponding Sections below. This recursion is performed until $Ng = 3000$. The Np and Ng values are justified in the parameter fine-tuning revealed in Section 3.1.
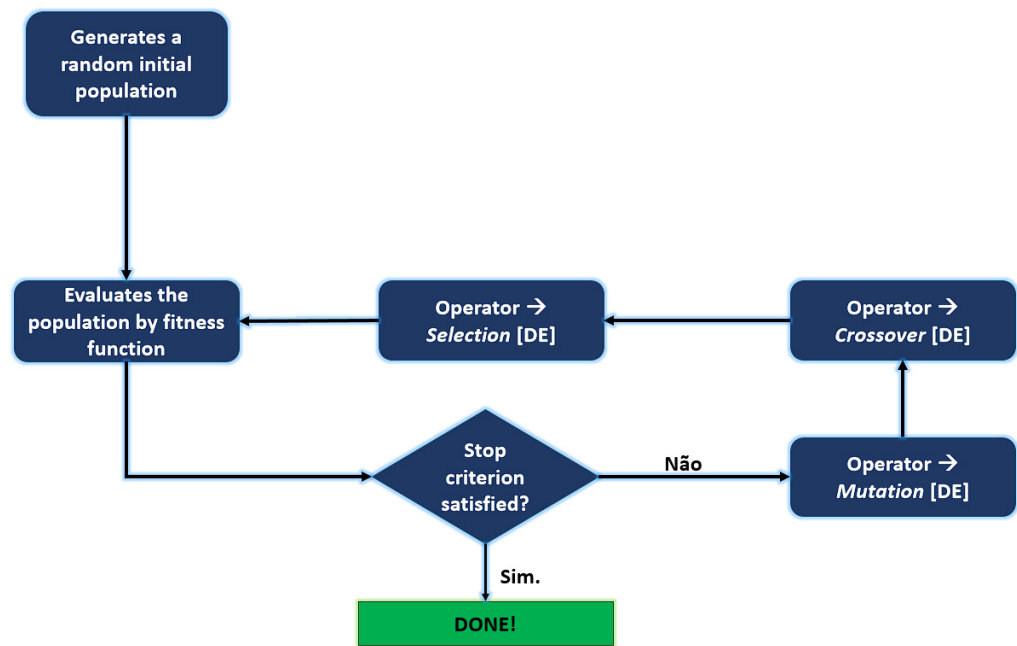
Figure 5. Flowchart for DE.

Finally, the individual of the last generation with the lowest fitness value is determined. The individual's information will be the parameters that the algorithm needs to find.

Mutation Operator for DE

For each target vector $\phi_{i,G}$, com $i = 1, \ldots, N_P$, a new vector is generated through Equation (13) [40].

$$v_{i,G+1} = \phi_{rr1,G} + 0,5(\phi_{rr3,G} - \phi_{rr2,G}) \tag{13}$$

where $rr1, rr2, rr3 \in \{1, 2, ..., N_P\}$ are mutually distinct items and also different from index i.

At the end of the mutation process, the matrix of mutated individuals is obtained, in which each individual is given by $v_{i,G+1}$ with $i = 1, \ldots, N_P$.

Crossover Operator for DE

Let $\phi_{i,G}$ be the target vector under analysis and $v_{i,G+1}$ the respective mutated vector, obtained by Equation (13). The vector $u_{i,G+1} = (u_{1i,G+1}, u_{2i,G+1}, \ldots, u_{MMi,G+1})$ is called a trial vector and is obtained as follows.

$$u_{ji,G+1} \begin{cases} u_{ji,G+1}, & \text{if } r_j \leq CR \text{ or } j = I_i \\ \phi_{ji,G}, & \text{if } r_j > CR \text{ and } j \neq I_i \end{cases}$$

where $j = 1, \ldots, M$, $r_j \sim (0,1)$, $CR \in [0,1]$ is a constant that defines the rate of *crossover* and Ii is a randomly chosen index $\in \{1, \ldots, M\}$ [40].

Selection Operator for DE

$\phi_{i,G}$ is the target vector under analysis and $u_{i,G+1}$ is its respective trial vector. The selection operator of the differential evolution is conducted as follows:

If $u_{i,G+1}$ has a fitness value greater than the fitness value of $\phi_{i,G}$, then $\phi_{i,G+1} = u_{i,G+1}$; Else, $\phi_{i,G+1} = \phi_{i,G}$.

At the end of the selection process, the new population is acquired, formed by the target vectors $\phi_{i,G+1}$, com $i = 1, \ldots, Np$.

Finally, integrating the selection, crossover, and mutation operators the way it was previously described in the Figure 5 flowchart, we have the standard version of the Differ-

ential Evolution Algorithm known by the notation DE/rand/1/bin (for details of other variants, see [43,44].

2.4. Plot of I vs. V Curve

With parameters found in the reference conditions, the I_L values can be updated for any temperature and irradiation values by Equation (14) [45].

$$I_L = \left(\frac{G}{G_{ref}} \right) \left(I_{L,ref+} \mu_{ISC} \left(T_c - T_{c,ref} \right) \right) \tag{14}$$

where G is the solar irradiance (W/m^2) and μ_{ISC} is the short-circuit current temperature coefficient.

The values of the reverse saturation current of the diode (I_0, I_1 and I_2), can also be updated to the desired values through Equation (15) [45].

$$I_0 = I_{0,ref} \left(\frac{T_C}{T_{C,ref}} \right)^3 exp \left[\left(\frac{q e_g}{kA} \right) \left(\frac{1}{T_{c,ref}} - \frac{1}{Tc} \right) \right] \tag{15}$$

Where e_g is the diode diffusion factor (V), μ_{ISC} is the short-circuit current temperature coefficient, and μ_{ISC} is the short-circuit current temperature coefficient.

The value of the parameter R_{sh} varies proportionally with the irradiance value, according to Equation (16) [46]. In contrast, in this method, the A, $A1$, $A2$, and Rs values remain constant.

$$R_{sh} = R_{shref} \left(\frac{G_{ref}}{G} \right) \tag{16}$$

In this way, it is possible to obtain the I $\times$ V curve of the module, through Equation (2), for the 1D5P case or through Equation (4), for the 2D7P model, thus determining the currents, voltages, and output powers of the photovoltaic module for the conditions desired.

The implementation of the algorithms to obtain the parameters and the plot of the curves were carried out using the MATLAB™ software [47].

3. Results and Discussions

As seen in Section 2 of this research, bio-inspired algorithms extract the necessary parameters from the models in the reference conditions. Thus, Table 2 shows the values of the parameters found by the Particle Swarm Optimization, Genetic Algorithm, and Differential Evolution Algorithm algorithms for the 1D5P and 2D7P models of the CANADIAN CS-3W-450-MS solar module [22].

Table 2. Parameters extracted by each method from the CANADIAN CS-3W-450-MS module.

	I_{01}	Rs	$A1$	Rsh	I_L	I_{02}	$A2$
PSO 1D5P	1.83×10^{-7}	3.151×10^{-3}	1.555148	3581	11.605	--	--
PSO 2D7P	1.00×10^{-8}	2.77×10^{-9}	1.993292	4146.44	11.605	4.998×10^{-7}	1.64692
GA 1D5P	7.62×10^{-7}	4.123×10^{-3}	1.688376	4999.98	11.702	--	--
GA 2D7P	1.00×10^{-6}	2.607×10^{-2}	1.7909	4999.99	11.820	$1.00.10^{-6}$	1.7925
DE 1D5P	2.83×10^{-8}	7.085×10^{-2}	1.408829	3045.88	11.60537	--	--
DE 2D7P	3.387×10^{-7}	5.22×10^{-3}	1.785252	4059.22	11.6051	7.32×10^{-8}	1.49564

With the extracted parameters, it is possible to modify them for any values of temperature and irradiation with the auxiliary equations presented in Section 2.4 of this research. Thus, it is possible to simulate the I–V curves for the desired situations.

In order to verify the effectiveness of the algorithms, simulations were carried out in five different situations: The first situation is performed under STC conditions, the second occurs with $G = 700$ W/m^2 and $Tc = 40$ °C, the third with $G = 400$ W/m^2 and

$Tc = 60\ °C$, the fourth with $G = 1050\ \mathrm{W/m^2}$ and $Tc = 20\ °C$, and finally, the Nominal Operating Cell Temperature (NOMT) with $G = 800\ \mathrm{W/m^2}$ and $Tc \cong 44\ °C$. According to [13], the first three cases represent very different operating conditions and cover a relevant range of these variables, as it changes from a pessimistic case, with low irradiation and high-temperature values, to average irradiation and temperature values in the cell, which are most commonly encountered in practice and arrive in the STC situation. In addition to these three simulations, a last but one was performed with irradiation values higher than the STCs. In comparison, the temperature values in the cell are lower than those of the standard test conditions. According to [24], this scenario would have higher electrical currents and power than the STCs, which makes this circumstance important to be analyzed. Although these conditions are difficult to locate around the globe, it is possible to find them in some regions of Brazil [48,49]. And finally, the last one is the case with the NOMT conditions, which are common conditions to find [50] and whose function is to validate the effectiveness of the employed schemes in usual situations.

Figure 6a shows the superposition of the curves generated by the bio-inspired algorithms PSO, GA, and DE using the 1D5P model, while Figure 6b reveals the curves using the 2D7P model, under reference conditions (STC). Both curves present the data provided by CANADIAN SOLAR for comparison purposes. Table 3 indicates the points of $(V_{0Cref}, 0)$, (V_{MPref}, I_{MPref}), $(0, I_{SCref})$ and the average relative error $(e\%)$ of the data obtained by the parameters in relation to those provided by the manufacturer. The relative percentage error $(e\%)$ is calculated by Equation (17), while the maximum power point P_{MP} is found by the product of the current I_{MP} by the voltage V_{MP}.

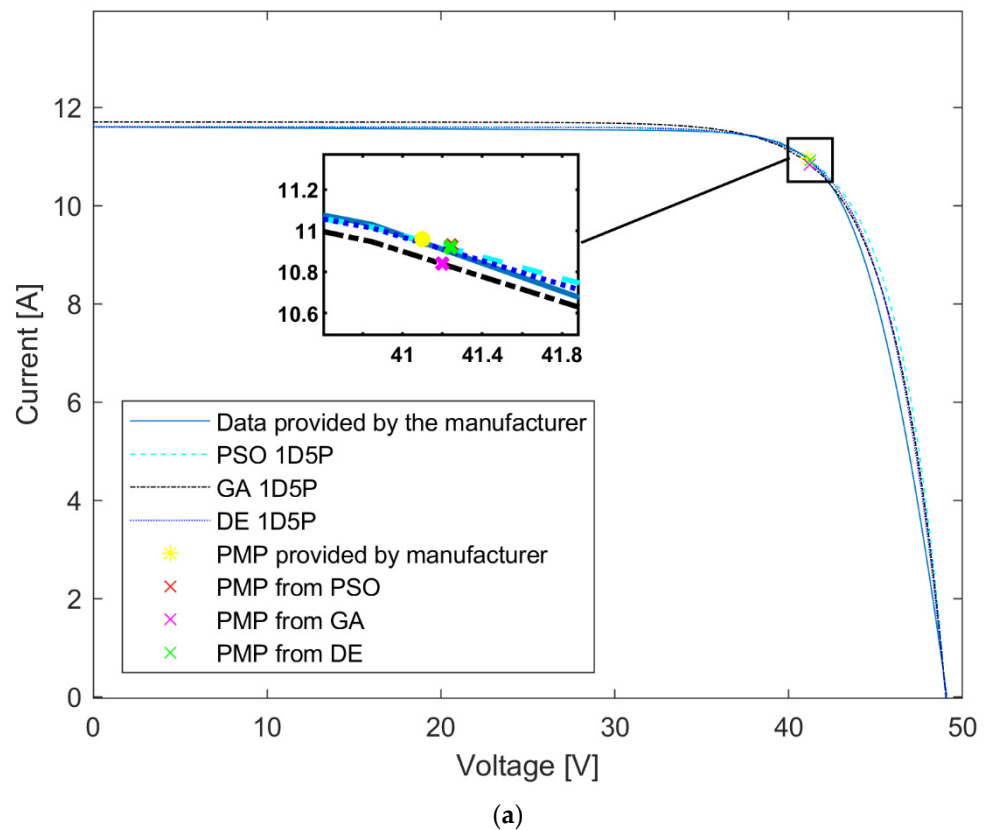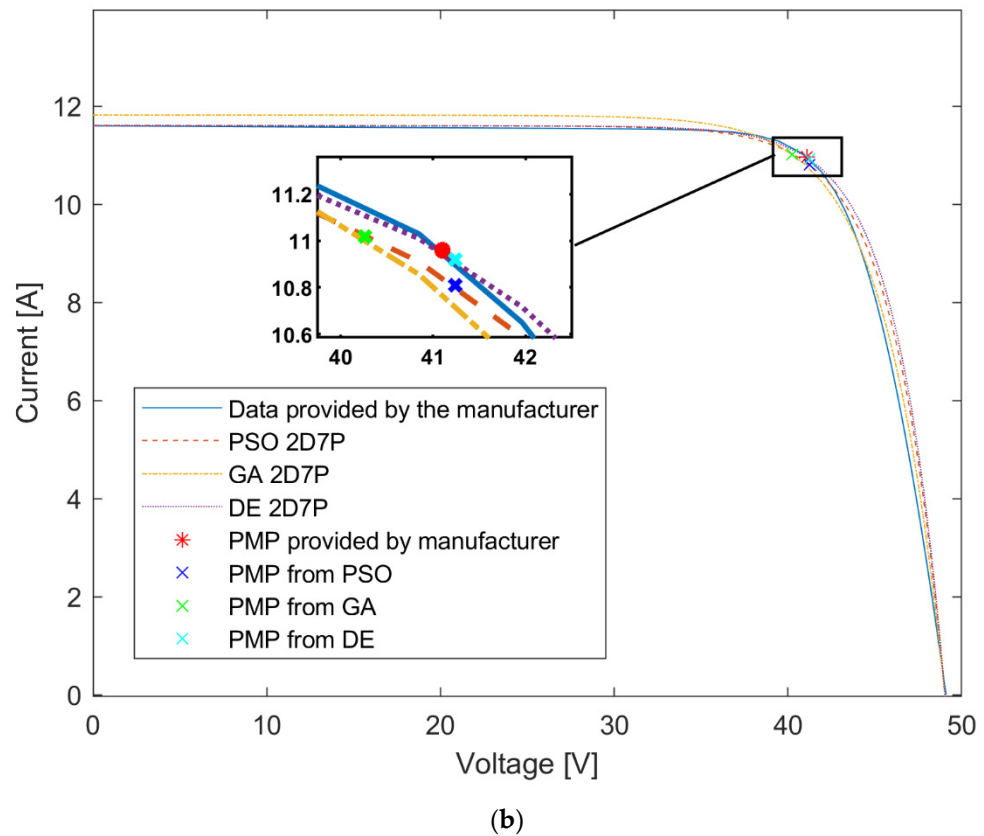$$e\% = \left| \frac{value_{data} - value_{simulated}}{value_{data}} \right| \times 100\% \tag{17}$$

(**a**)

Figure 6. *Cont.*

(**b**)

Figure 6. Superposition of I × V curves generated by PSO, GA, and DE for (**a**) 1D5P and (**b**) 2D7P under conditions G = 1000 W/m² and Tc = 25 °C.

Table 3. Points of interest for the different methods under STC conditions G = 1000 W/m² and Tc = 25 °C.

Method	P_{MP}	I_{MP}	V_{MP}	I_{SC}	V_{OC}
Data provided by Manufacture	450.456 W	10.960 A	41.100 V	11.600 A	49.100 V
PSO 1D5P e%	450.632 W <0.10%	10.926 A 0.31%	41.244 V 0.35%	11.600 A <0.10%	49.038 V 0.13%
GA 1D5P e%	449.904 W 0.12%	10.920 A 0.36%	41.200 V <0.10%	11.600 A <0.10%	49.038 V 0.13%
DE 1D5P e%	450.341 W <0.10%	10.920 A 0.36%	41.240 V 0.34%	11.600 A <0.10%	49.040 V 0.12%
PSO 2D7P e%	445.804 W 1.03%	10.810 A 1.37%	41.240 V 0.34%	11.605 A <0.10%	49.030 V 0.14%
GA 2D7P e%	443.544 W 1.53%	11.017 A 0.52%	40.260 V 2.00%	11.820 A 1.89%	49.037 V 0.13%
DE 2D7P e%	450.341 W <0.10%	10.920 A 0.36%	41.240 V 0.34%	11.605 A <0.10%	49.390 V 0.59%

Through Table 3, it is possible to verify that the simulations using the 1D5P model had significantly better results than those carried out in the 2D7P model. The methods applied to the 1D5P model had an average relative error of a maximum of 0.6%, whereas those applied to the 2D7P model had errors of up to 2%. It is evident that the order of the model affects the estimates of the model parameters. This can be explained by the fact that the algorithms need to find seven variables in the 2D7P model compared to five in

the 1D5P model. At the same time, the fitness function only has three points to evaluate due to the restriction of information on the operating curve of the modules declared by the manufacturer. Studies conducted by [19,20] point out that there is a tendency for bio-inspired algorithms to have greater simulation accuracy the greater the number of points in the evaluation criterion. Thus, the fact that the algorithms need to adjust two more variables in the 2D7P model may explain the lower performance.

Analyzing in a general way, the results were positive for the STC conditions. Since the worst case was at the maximum power voltage point by the GA 2D7P scheme showing $e\% = 2\%$. It is worth mentioning that the combinations with the best performance were the PSO 1D5P and DE 1D5P, which presented errors below 0.4% for the cases of P_{MP}, I_{SC}, and V_{OC}, in the STC conditions.

Similar to the previous case, Figures 7–9 show the superimposition of the curves generated by the bio-inspired algorithms and the data provided by CANADIAN SOLAR [22], under the specified conditions. Tables 4–6 show the points of interest $(V_{0C}, 0)$, (V_{MP}, I_{MP}), and $(0, I_{SC})$ as well as the respective relative errors of each method. It is important to emphasize that the data provided by CANADIAN SOLAR, except for the standard test conditions, are generated from simulations made in the PVSYST SOFTWARE [51].
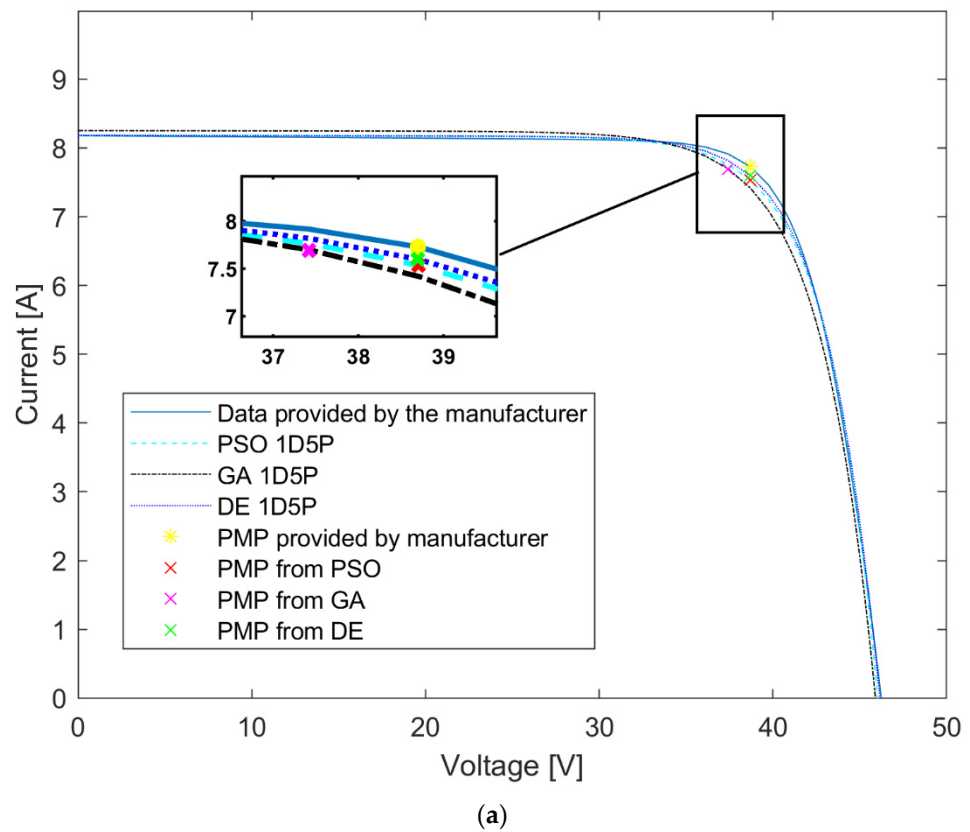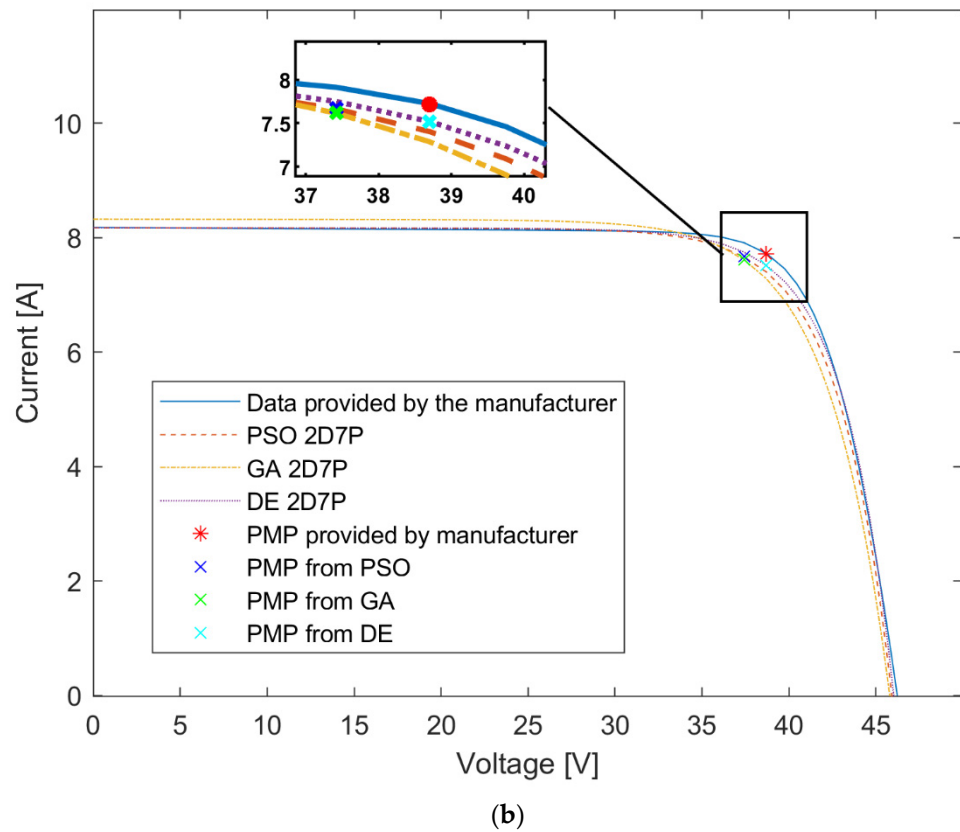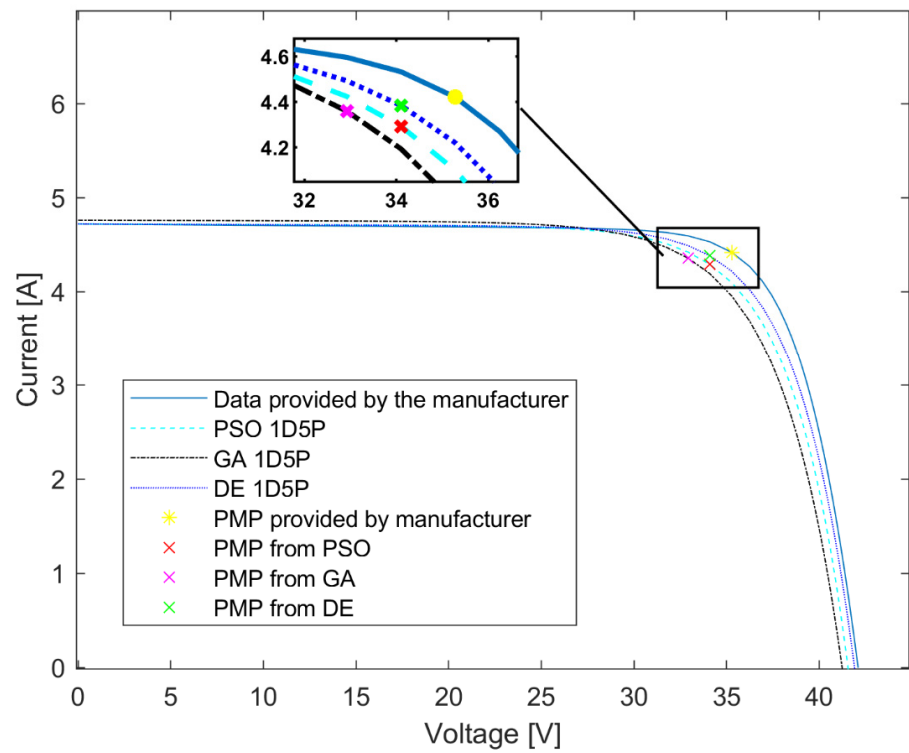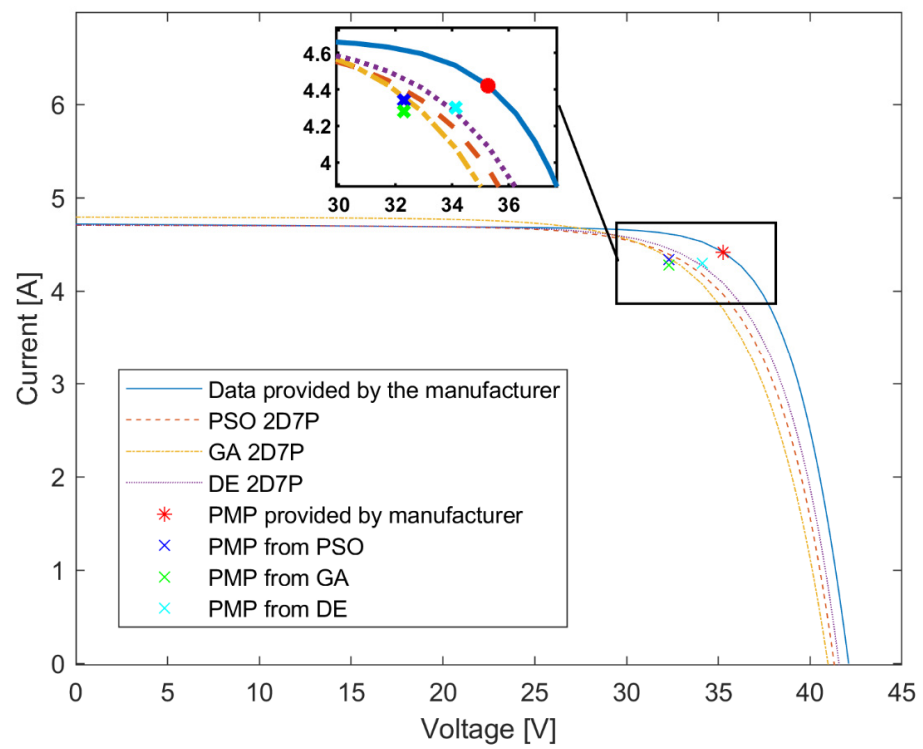

(**a**)

Figure 7. *Cont.*

(b)

Figure 7. Superposition of I × V curves generated by PSO, GA, and DE for (**a**) 1D5P and (**b**) 2D7P under conditions G = 700 W/m^2 and Tc = 40 °C.

Table 4. Points of interest for the different methods under conditions G = 700 W/m^2 and Tc = 40 °C.

Method	P_{MP}	I_{MP}	V_{MP}	I_{SC}	V_{OC}
Data provided by Manufacture	298.996 W	7.726 A	38.700 V	8.180 A	46.210 V
PSO 1D5P e%	291.492 W 2.51%	7.532 A 2.51%	38.700 V <0.10%	8.184 A <0.10%	46.050 V 0.34%
GA 1D5P e%	287.984 W 3.68%	7.696 A 0.39%	37.420 V 3.30%	8.253 A 0.88%	45.900 V 0.67%
DE 1D5P e%	294.120 W 1.63%	7.600 A 1.63%	38.700 V <0.10%	8.180 A <0.10%	46.180 V <0.10%
PSO 2D7P e%	286.637 W 4.13%	7.660 A 0.85%	37.420 V 3.31%	8.174 A <0.10%	45.900 V 0.67%
GA 2D7P e%	284.968 W 4.69%	7.616 A 1.42%	37.417 V 3.31%	8.325 A 1.76%	42.800 V 7.37%
DE 2D7P e%	291.084 W 2.65%	7.520 A 2.67%	38.708 V <0.10%	8.174 A <0.10%	46.050 V 0.34%

(**a**)

(**b**)

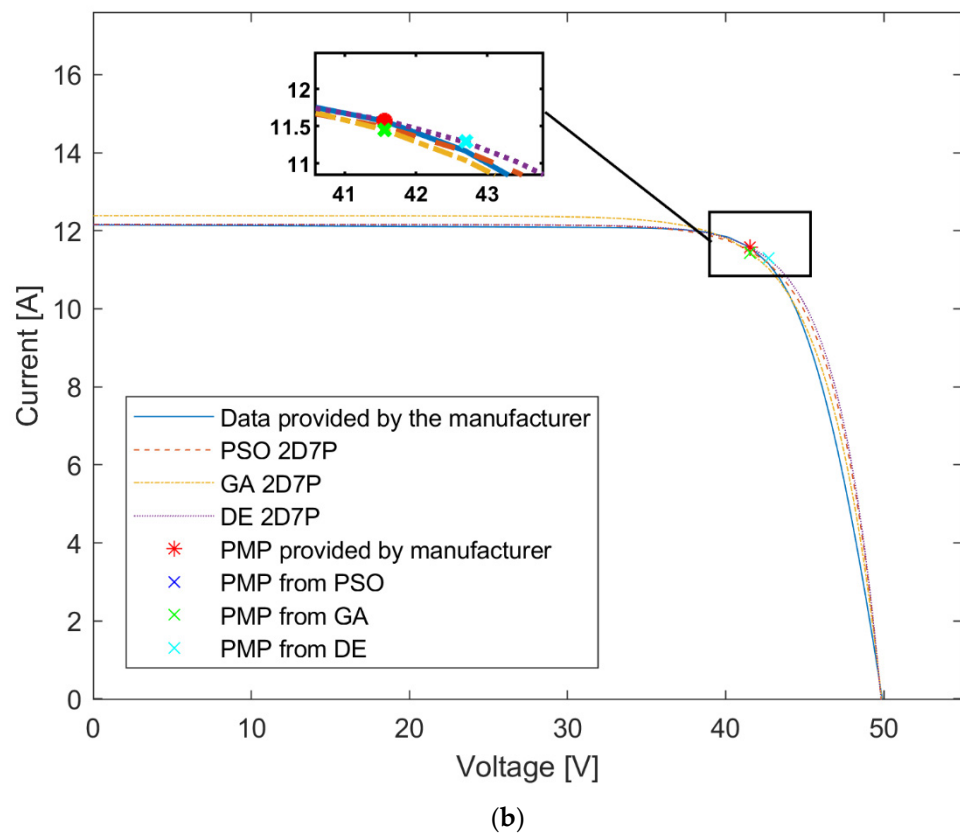**Figure 8.** Superposition of I × V curves generated by PSO, GA, and DE for (**a**) 1D5P and (**b**) 2D7P under conditions G = 400 W/m^2 and Tc = 60 °C.

Table 5. Points of interest for the different methods under conditions G = 400 W/m^2 and Tc = 60 $^\circ$C.

Method	P_{MP}	I_{MP}	V_{MP}	I_{SC}	V_{OC}
Data provided by Manufacture	155.893 W	4.420 A	35.270 V	4.720 A	42.100 V
PSO 1D5P	147.187 W	4.310 A	34.150 V	4.7230 A	41.650 V
e%	5.58%	2.50%	3.17%	<0.1%	1.06%
GA 1D5P	143.575 W	4.360 A	32.930 V	4.762 A	41.260 V
e%	7.90%	1.36%	6.63%	0.90%	2.00%
DE 1D5P	150.260 W	4.400 A	34.150 V	4.720 A	41.920 V
e%	3.61%	0.45%	3.17%	<0.10%	0.43%
PSO 2D7P	142.960 W	4.340 A	32.940 V	4.710 A	41.300 V
e%	8.30%	1.81%	6.61%	0.21%	1.90%
GA 2D7P	140.940 W	4.280 A	32.930 V	4.800 A	41.000 V
e%	9.59%	3.17%	6.63%	1.69%	2.61%
DE 2D7P	146.716 W	4.300 A	34.120 V	4.710 A	41.600 V
e%	5.88%	2.71%	3.26%	0.21%	1.18%

(**a**)

Figure 9. *Cont.*

(**b**)

Figure 9. Superposition of I × V curves generated by PSO, GA, and DE for (**a**) 1D5P and (**b**) 2D7P under conditions G = 1050 W/m^2 and Tc = 20 °C.

Table 6. Points of interest for the different methods under conditions G = 1050 W/m^2 and Tc = 20 °C.

Method	P_{MP}	I_{MP}	V_{MP}	I_{SC}	V_{OC}
Data provided by Manufacture	480.849 W	11.570 A	41.560 V	12.150 A	49.910 V
PSO 1D5P	482.141 W	11.294 A	42.690 V	12.150 A	49.830 V
e%	0.27%	2.40%	2.71%	<0.10%	0.16%
GA 1D5P	479.017 W	11.525 A	41.564 V	12.250 A	49.850 V
e%	0.38%	0.39%	<0.10%	0.82%	0.12%
DE 1D5P	480.817 W	11.568 A	41.564 V	12.150 A	49.810 V
e%	<0.10%	<0.10%	<0.10%	<0.10%	0.20%
PSO 2D7P	477.471 W	11.488 A	41.564 V	12.160 A	49.835 V
e%	0.70%	0.71%	<0.10%	<0,10%	0.15%
GA 2D7P	475.908 W	11.450 A	41.564 V	12.380 A	49.830 V
e%	1.03%	1.04%	<0.10%	1.89%	0.16%
DE 2D7P	481.885 W	11.288 A	42.690 V	12.160 A	49.870 V
e%	0.22%	2.44%	2.72%	<0.10%	<0.10%

Observing Figures 7–9, as well as their respective tables, it can be seen that the model linked to the most successful method was DE 1D5P. It showed relative errors of less than 0.2% for the case of $G = 1050$ W/m^2 and $Tc = 20$ °C, less than 1.63% for the case of $G = 700$ W/m^2 and $Tc = 40$ °C, and less than 3.61% in the case of low irradiation. The algorithms that used the 1D5P model also showed good results, emphasizing the PSO 1D5P scheme, which presented a maximum relative error of approximately 5% for the worst case, which was the one with the lowest irradiation.

Another important piece of information is that the more the conditions deviated from the STC conditions, the greater the error. This happens because the reference parameters are collected through the datasheet under STC conditions. However, even choosing a very pessimistic condition, $G = 400\,\text{W/m}^2$ and $Tc = 60\,°\text{C}$, which is practically one of the worst possible conditions to be found in practice, the schemes DE 1D5P, PSO 1D5P, GA 1D5P, and DE 2D7P showed errors less than 8%. The study by [26], which tested several modeling processes and the extraction of photovoltaic module parameters, intended to verify the effectiveness and precision of each of the methods and resulted in Chenni's method [45], was the most accurate, and [13], who compared Chenni's method with PSO 1D5P, revealed that this error range is acceptable for simulating photovoltaic modules.

In this work, the 2D7P and GA 2D7P combinations presented errors greater than 8%. Thus, their use is less recommended than the other schemes presented.

To complete all cited cases, Figure 10a shows the superposition of the curves generated by the bio-inspired algorithms PSO, GA, and DE using the 1D5P model, while Figure 10b reveals the curves using the 2D7P model under NOMT conditions. Table 7 show the points of interest $(V_{0C}, 0)$, (V_{MP}, I_{MP}), and $(0, I_{SC})$ as well as the respective relative errors of this case. It is important to highlight that the NOMT conditions are $G = 800\,\text{W/m}^2$, $T_{ambience} = 20\,°\text{C}$, and wind speed ($W_s$) equals 1.5 m/s. According to [52] the cell temperature of a photovoltaic module can be described by Equation (18).

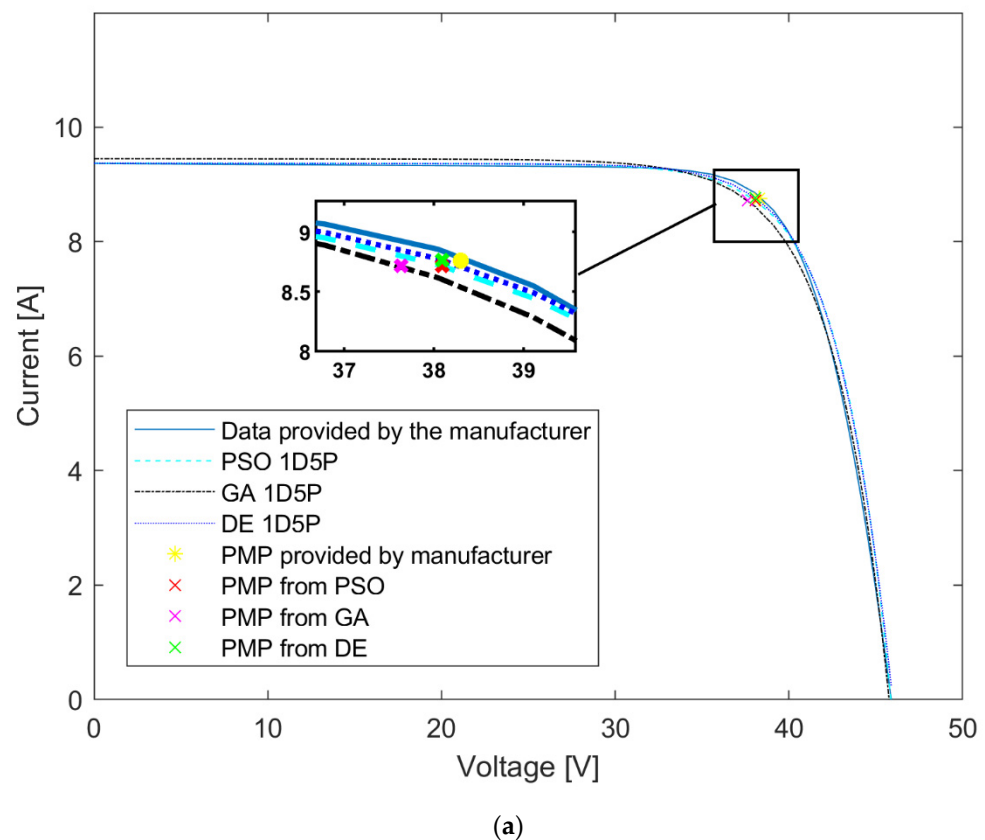$$T_c = 0.943 \times T_{ambience} + 0.028 \times G - 1.528 \times W_s + 4.3 \tag{18}$$
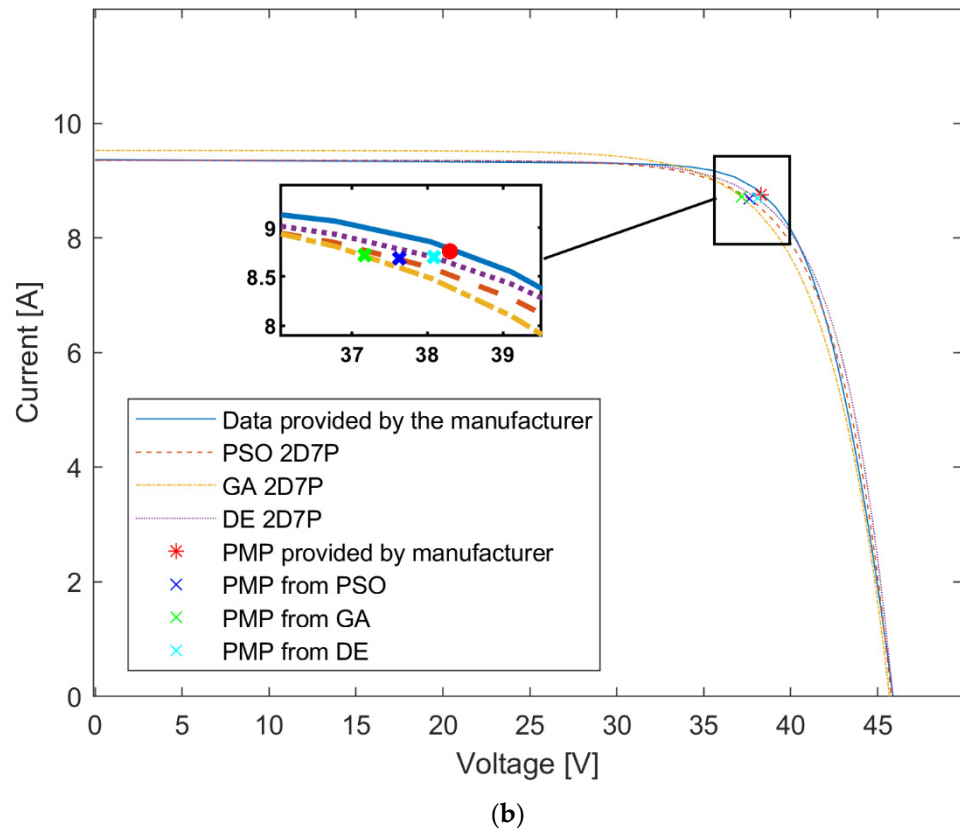

(a)

Figure 10. *Cont.*

Figure 10. Superposition of I × V curves generated by PSO, GA, and DE for (**a**) 1D5P and (**b**) 2D7P under conditions G = 800 W/m^2 and Tc ≅ 44 °C.

Table 7. Points of interest for the different methods under NOMT conditions G = 800 W/m^2 and Tc ≅ 44 °C.

Method	P_{MP}	I_{MP}	V_{MP}	I_{SC}	V_{OC}
Data provided by Manufacture	336.00 W	8.760 A	38.300 V	9.360 A	46.200 V
PSO 1D5P e%	331.980 W 1.20%	8.716 A 0.50%	38.088 V 0.55%	9.372 A 0.13%	45.780 V 0.91%
GA 1D5P e%	325.058 W 3.26%	8.718 A 0.48%	37.630 V 1.75%	9.450 A 0.96%	45.680 V 1.13%
DE 1D5P e%	333.850 W 0.64%	8.765 A <0.10%	38.089 V 0.55%	9.372 A 0.13%	45.880 V 0.69%
PSO 2D7P e%	326.854 W 2.72%	8.686 A 0.84%	37.630 V 1.75%	9.358 A <0.10%	45.770 V 0.93%
GA 2D7P e%	324.131 W 3.53%	8.720 A 0.46%	37.171 V 2.95%	9.530 A 1.82%	45.665 V 1.16%
DE 2D7P e%	331.222 W 1.42%	8.696 A 0.73%	38.089 V 0.55%	9.358 A <0.10%	45.860 V 0.74%

Analyzing Figure 10 and Table 7, it can be seen that all combinations are viable for this case since the highest relative error was 3.53%. Analogous to all previous cases, the most successful schemes were PSO 1D5P, which presented a maximum relative error of 1.2%, and DE 1D5P, which presented errors of less than 0.7%. This last result proves that the methods used in this research are efficient for extracting the parameters and simulating

the photovoltaic modules. Then, in a situation usually found, all the schemes had a relative error of less than 4%. In addition, the DE 1D5P method reached a higher level than the others and had an accuracy greater than 99% for this case.

3.1. Sensitivity Analysis of the Fitness Function

According to Section 2, the more the fitness function value approaches zero, the more the parameters are adjusted to the model. Thus, the requirements for choosing Np and Ng were that, as a priority, the calculated value of the function (ff) should be at most 10^{-2}. However, if there is no aptitude convergence in up to 2 s, the chosen parameters are those that originated the smallest value of ff up to 2 s. Table 8 reveals the fitness values for different Np and Ng values and summarizes the search for more adequate values for each simulation scheme carried out in the research (parameter fine-tuning). The computer used for testing has an AMD Ryzen 5 3600X 6-Core Processor 3.80 GHz and 16 GB of RAM. It is noteworthy that the absolute time is not relevant to the study. It only serves as a benchmark to superficially compare the cost of the three employed methods.

Table 8. Sensitivity of fitness function.

	Np	Ng	ff	Time (s)
PSO 1D5P	30	300	0.3	0.04
	50	300	0.00401	0.058
	30	1000	0.00438	0.07
	50	1000	5.75×10^{-6}	0.121
PSO 2D7P	10	100	0.18	0.098
	50	100	0.04	0.048
	30	1000	0.36	0.24
	50	1000	0.00426	0.28
GA 1D5P	10	100	2.83	0.06
	50	100	0.51	0.0965
	10	2000	0.82778	0.24
	50	3000	0.06	1.8
GA 2D7P	10	100	1.76	0.068
	50	100	0.33	0.012
	10	1000	0.36	0.2
	50	3000	0.09	2
DE 1D5P	10	100	2.26	0.01
	50	100	0.06	0.07
	10	300	0.56	0.06
	50	300	0.001	0.12
DE 2D7P	10	100	0.389	0.06
	50	100	0.0022	0.008
	10	300	0.36	0.074
	50	300	6×10^{-6}	0.14

Analyzing the performances of each method, as well as the algorithm's time to find the parameters, it is observed that the DE 1D5P scheme obtained the best results in this work because it was the one that presented the highest accuracy in the points of interest in the most distant conditions from the STC, in addition to having presented precise results in this reference condition, with errors of less than 0.2%. In addition, it was the method with the shortest processing time to obtain the parameters.

Analogously to the study for the module made up of monocrystalline cells in Section 3 of this work, research was carried out for the module CANADIAN CS-3W-440-P [53] made up of polycrystalline cells. The results obtained were remarkably similar for both cases. This detailed study is available in the Supplementary Materials.

4. Conclusions

This work applied the bio-inspired algorithms PSO, GA, and DE in the extraction of the parameters of the circuit equivalent to a photovoltaic module in the 1D5P and 2D7P models to simulate the I-V characteristic curves for any irradiation and temperature scenarios, only using the information contained in the module datasheet. In addition, a comparison was made between the results obtained from each method with data provided by the CANADIAN module manufacturer in different irradiation and temperature scenarios.

In general, the bio-inspired algorithm that presented the highest accuracy was the DE, with maximum relative errors of 0.4% in conditions close to the reference, 3.61% for scenarios very distant from the reference, and 1.61% for intermediate situations, when using the model 1D5P; furthermore, it was the one that achieved the shortest time to estimate the parameters. The PSO algorithm achieved better results than the GA algorithm, mainly in cases where the temperature and irradiation conditions were quite different from the STC, in which the worst case had an error of approximately 5%. In comparison, the GA algorithm inaccurately measured 7.9% when using the 1D5P model. Therefore, the PSO achieves second place among the algorithms presented in this study.

One of the most relevant contributions of this research is the conclusion that using the 1D5P model leads to better results than those obtained using the 2D7P model. This occurs due to the fitness function's construction process, which uses only three points of the $I \times V$ curve in the reference conditions. This scarcity of data, linked to the fact that the two-diode model needs to find two more parameters than the single-diode model and, therefore, is also more flexible, are the main reasons the single-diode model stands out. However, it is worth noting that by conducting the fitness function as presented in Section 2, it is possible to extract the model parameters and, posteriorly, simulate the $I \times V$ curves for the desired temperature and irradiation conditions for any commercial photovoltaic module, using only its respective datasheet, without needing external studies or measurements.

Finally, it is concluded that the PSO 1D5P and, mainly, DE 1D5P schemes presented favorable results for extracting parameters and, consequently, performing the simulation of photovoltaic modules with excellent accuracy through the precise generation of $I \times V$ curves. Furthermore, these schemes demonstrate remarkable viability and robustness, as they achieve excellent accuracy while requiring minimal processing time and no external data beyond the technical datasheet of the photovoltaic module.

Conflicts of Interest: The authors declare no conflict of interest.

References

1. Haegel, N.M.; Atwater, H.; Barnes, T.; Breyer, C.; Burrell, A.; Chiang, Y.-M.; De Wolf, S.; Dimmler, B.; Feldman, D.; Glunz, S.; et al. Terawatt-scale photovoltaics: Transform global energy. *Science* **2019**, *364*, 836–838. [CrossRef] [PubMed]
2. Kurbatova, T.; Perederii, T. Global trends in renewable energy development. In Proceedings of the 2020 IEEE KhPI Week on Advanced Technology (KhPIWeek), Kharkiv, Ukraine, 5 October 2020; pp. 260–263. [CrossRef]
3. Almeida, E.L.; Andrade, C.M.G.; Andreo Dos Santos, O. Production of Biodiesel Via Catalytic Processes: A Brief Review. *Int. J. Chem. React. Eng.* **2018**, *16*, 20170130. [CrossRef]
4. Freitas, H.; Olivo, J.; Andrade, C. Optimization of Bioethanol In Silico Production Process in a Fed-Batch Bioreactor Using Non-Linear Model Predictive Control and Evolutionary Computation Techniques. *Energies* **2017**, *10*, 1763. [CrossRef]
5. Nwaigwe, K.N. Assessment of wind energy technology adoption, application and utilization: A critical review. *Int. J. Environ. Sci. Technol.* **2022**, *19*, 4525–4536. [CrossRef]
6. Alhmoud, L. Why Does the PV Solar Power Plant Operate Ineffectively? *Energies* **2023**, *16*, 4074. [CrossRef]
7. IRENA. International Renewable Energy Agency. Capacity and Generation PV Data. 2023. Available online: https://www.irena.org/Data/View-data-by-topic/Capacity-and-Generation/Technologies (accessed on 1 August 2023).
8. IEA. International Energy Agency. Renewables 2021—Analysis and Forecast to 2026. 2021. Available online: https://iea.blob.core.windows.net/assets/5ae32253-7409-4f9a-a91d-1493ffb9777a/Renewables2021-Analysisandforecastto2026.pdf (accessed on 1 August 2023).
9. Da Rocha Queiroz, J.; Da Silva Souza, A.; Gussoli, M.K.; De Oliveira, J.C.D.; Andrade, C.M.G. Construction and Automation of a Microcontrolled Solar Tracker. *Processes* **2020**, *8*, 1309. [CrossRef]
10. Tifidat, K.; Maouhoub, N.; Askar, S.S.; Abouhawwash, M. Numerical procedure for accurate simulation of photovoltaic modules performance based on the identification of the single-diode model parameters. *Energy Rep.* **2023**, *9*, 5532–5544. [CrossRef]
11. Chin, V.J.; Salam, Z.; Ishaque, K. Cell modelling and model parameters estimation techniques for photovoltaic simulator application: A review. *Appl. Energy* **2015**, *154*, 500–519. [CrossRef]
12. Laudani, A.; Riganti Fulginei, F.; Salvini, A. High performing extraction procedure for the one-diode model of a photovoltaic panel from experimental I–V curves by using reduced forms. *Sol. Energy* **2014**, *103*, 316–326. [CrossRef]
13. Provensi, L.L.; Grala, G.H.; Zukeram Junior, E.S.; Alcantara, G.P.; Krummenauer, R.; Andrade, C.M.G. Modeling of the operating characteristics of photovoltaic modules based on particle swarm optimization. *Env. Prog Sustain. Energy* **2022**, *41*, e13831. [CrossRef]
14. Abbassi, A.; Ben Mehrez, R.; Touaiti, B.; Abualigah, L.; Touti, E. Parameterization of photovoltaic solar cell double-diode model based on improved arithmetic optimization algorithm. *Optik* **2022**, *253*, 168600. [CrossRef]
15. Chin, V.J.; Salam, Z.; Ishaque, K. An accurate modelling of the two-diode model of PV module using a hybrid solution based on differential evolution. *Energy Convers. Manag.* **2016**, *124*, 42–50. [CrossRef]
16. Ibrahim, I.A.; Hossain, M.J.; Duck, B.C. A hybrid wind driven-based fruit fly optimization algorithm for identifying the parameters of a double-diode photovoltaic cell model considering degradation effects. *Sustain. Energy Technol. Assess.* **2022**, *50*, 101685. [CrossRef]
17. Koohi-Kamali, S.; Rahim, N.A.; Mokhlis, H.; Tyagi, V.V. Photovoltaic electricity generator dynamic modeling methods for smart grid applications: A review. *Renew. Sustain. Energy Rev.* **2016**, *57*, 131–172. [CrossRef]
18. Yahya-Khotbesara, A.; Shahhoseini, A. A fast modeling of the double-diode model for PV modules using combined analytical and numerical approach. *Solar Energy* **2018**, *162*, 403–409. [CrossRef]
19. Liang, J.; Ge, S.; Qu, B.; Yu, K.; Liu, F.; Yang, H.; Wei, P.; Li, Z. Classified perturbation mutation based particle swarm optimization algorithm for parameters extraction of photovoltaic models. *Energy Convers. Manag.* **2020**, *203*, 112138. [CrossRef]
20. Reis, L.R.d.D. *Determinação de Parâmetros de Módulos Fotovoltaicos Utilizando o Método de Newton Raphson e Algoritmos Genéticos*; Universidade Federal de Uberlândia: Uberlândia, Brazil, 2018. [CrossRef]
21. Yousri, D.; Allam, D.; Eteiba, M.B.; Suganthan, P.N. Static and dynamic photovoltaic models' parameters identification using Chaotic Heterogeneous Comprehensive Learning Particle Swarm Optimizer variants. *Energy Convers. Manag.* **2019**, *182*, 546–563. [CrossRef]

22. Canadian Solar. *Canadian Solar HiKu 450Wp MS Module Datasheet*; Canadian Solar: Guelph, ON, Canada, 2019. Available online: https://www.canadiansolar.com/wp-content/uploads/2019/12/Canadian_Solar-Datasheet-HiKu_CS3W-MS_EN.pdf (accessed on 2 May 2023).

23. Kwak, J.I.; Nam, S.-H.; Kim, L.; An, Y.-J. Potential environmental risk of solar cells: Current knowledge and future challenges. *J. Hazard. Mater.* **2020**, *392*, 122297. [CrossRef]

24. Pinho, J.T.; Galdino, M.A. *Manual de Engenharia para Sistemas Fotovoltaicos*; Centro de Pesquisas de Energia Elétrica (CEPEL) and Centro de Referência para Energia Solar e Eólica Sérgio Brito (CRESESB): Rio de Janeiro, Brazil, 2014.

25. Gholami, A.; Ameri, M.; Zandi, M.; Gavagsaz Ghoachani, R. A single-diode model for photovoltaic panels in variable environmental conditions: Investigating dust impacts with experimental evaluation. *Sustain. Energy Technol. Assess.* **2021**, *47*, 101392. [CrossRef]

26. Aoun, N.; Bailek, N. Evaluation of mathematical methods to characterize the electrical parameters of photovoltaic modules. *Energy Convers. Manag.* **2019**, *193*, 25–38. [CrossRef]

27. Villalva, M.G.; Gazoli, J.R.; Filho, E.R. Comprehensive Approach to Modeling and Simulation of Photovoltaic Arrays. *IEEE Trans. Power Electron.* **2009**, *24*, 1198–1208. [CrossRef]

28. Zhang, F.; Wu, M.; Hou, X.; Han, C.; Wang, X.; Liu, Z. The analysis of parameter uncertainty on performance and reliability of photovoltaic cells. *J. Power Sources* **2021**, *507*, 230265. [CrossRef]

29. Ye, M.; Wang, X.; Xu, Y. Parameter extraction of solar cells using particle swarm optimization. *J. Appl. Phys.* **2009**, *105*, 094502. [CrossRef]

30. Lidaighbi, S.; Elyaqouti, M.; Ben Hmamou, D.; Saadaoui, D.; Assalaou, K.; Arjdal, E. A new hybrid method to estimate the single-diode model parameters of solar photovoltaic panel. *Energy Convers. Manag. X* **2022**, *15*, 100234. [CrossRef]

31. Chan, D.S.H.; Phang, J.C.H. Analytical methods for the extraction of solar-cell single- and double-diode model parameters from I–V characteristics. *IEEE Trans. Electron. Devices.* **1987**, *34*, 286–293. [CrossRef]

32. Kennedy, J.; Eberhart, R. Particle Swarm Optimization. In Proceedings of the IEEE International Conference, Whistler, BC, Canada, 17–22 September 1995; p. 7.

33. Clerc, M.; Kennedy, J. The particle swarm—Explosion, stability, and convergence in a multidimensional complex space. *IEEE Trans. Evol. Comput.* **2002**, *6*, 58–73. [CrossRef]

34. Holland, J.H. *Adaptation in Natural and Artificial Systems*; University of Michigan Press: Ann Arbor, MI, USA, 1975.

35. Back, T. Selective pressure in evolutionary algorithms: A characterization of selection mechanisms. In Proceedings of the First IEEE Conference on Evolutionary Computation, IEEE World Congress on Computational Intelligence, Orlando, FL, USA, 27–29 June 1994; IEEE: Piscataway, NJ, USA; pp. 57–62. [CrossRef]

36. Goldberg, D.E.; Deb, K. A Comparison of Selection Schemes Used in Genetic Algorithms. In *Foundations of Genetic Algorithms*; Rawlins, G.J.E., Ed.; Morgan Kaufmann: Burlington, MA, USA, 1991; pp. 69–93.

37. Holland, J.H. *Adaptation in Natural and Artificial Systems*, 2nd ed.; The MIT Press: Cambridge, MA, USA, 1992.

38. Michalewicz, Z. *Genetic Algorithms + Data Structures = Evolution Programs*, 3rd ed.; Springer: Charlotte, NC, USA, 1996.

39. Fogarty, T.C. Varying the Probability of Mutation in the Genetic Algorithm. In Proceedings of the Third International Conference on Genetic Algorithms; 1989; pp. 104–109.

40. Boccato, L.; Krummenauer, R.; Attux, R.; Lopes, A. Application of natural computing algorithms to maximum likelihood estimation of direction of arrival. *Signal Process.* **2012**, *92*, 1338–1352. [CrossRef]

41. Price, K.; Storn, R.M.; Lampinen, J.A. *Differential Evolution: A Practical Approach to Global Optimization (Natural Computing Series)*; Springer-Verlag: Berlin/Heidelberg, Germany, 2005.

42. Storn, R.; Price, K. Differential Evolution—A simple and efficient adaptive scheme for global optimization over continuous spaces. *J. Glob. Optim.* **1995**, *11*, 341–359. [CrossRef]

43. Das, S.; Suganthan, P.N. Differential Evolution: A Survey of the State-of-the-Art. *IEEE Trans. Evol. Computat.* **2011**, *15*, 4–31. [CrossRef]

44. Storn, R.; Price, K. Differential Evolution—A Simple and Efficient Heuristic for Global Optimization over Continuous Spaces. *J. Glob. Optim.* **1997**, *11*, 341–359. [CrossRef]

45. Chenni, R.; Makhlouf, M.; Kerbache, T.; Bouzid, A. A detailed modeling method for photovoltaic cells. *Energy* **2007**, *32*, 1724–1730. [CrossRef]

46. Pinto, C.S.B.S. *Validação Experimental do Modelo Cinco Parâmetros e Um Díodo de Painéis Fotovoltaicos (Dissertação)*; Técnico Lisboa: Lisboa, Portugal, 2016.

47. Mathworks, Matlab Software. Available online: https://www.mathworks.com/products/matlab.html (accessed on 2 May 2023).

48. Ministério da Agricultura e Pecuária, G.F. Instituto Nacional de Meteorologia. 2023. Available online: https://portal.inmet.gov.br/normais (accessed on 2 May 2023).

49. Ministério de Minas e Energia, C.; Centro de Referência para Energias Solar e Eólica Sérgio de S. Brito (CRESESB). 2023. Available online: http://www.cresesb.cepel.br/ (accessed on 2 May 2023).

50. Sun, V.; Asanakham, A.; Deethayat, T.; Kiatsiriroat, T. Evaluation of nominal operating cell temperature (NOCT) of glazed photovoltaic thermal module. *Case Stud. Therm. Eng.* **2021**, *28*, 101361. [CrossRef]

51. PVSYST. PVSYST Photovoltaic Software. 2023. Available online: https://www.pvsyst.com/ (accessed on 2 May 2023).

52. Tamizhmani, G.; Ji, L.; Tang, Y.; Petacci, L.; Osterwald, C. Photovoltaic Module Thermal/Wind Performance: Long-Term Monitoring and Model Development For Energy Rating. In Proceedings of the NCPV and Solar Program Review Meeting Proceedings, Denver, CO, USA, 24–26 March 2003; p. 4.

53. Canadian Solar. *Canadian Solar HiKu CS3W 440Wp Poly-Crystalline Datasheet*. 2020, p. 2. Available online: https://www.canadiansolar.com/test-au/wp-content/uploads/sites/2/2020/04/Canadian_Solar-Datasheet-HiKu_CS3W-P_v5.59_AU-2.pdf (accessed on 31 July 2023).